Magnetic characterisation of large grain, bulk Y-Ba-Cu-O superconductor-soft ferromagnetic alloy hybrid structures

M P Philippe [a,*], J-F Fagnard [a], S Kirsch [a], Z Xu [b], A R Dennis [b], Y-H Shi [b], D A Cardwell [b], B Vanderheyden [a] and P Vanderbemden [a]

[a] SUPRATECS and Department of Electrical Engineering and Computer Science (B28), University of Liège, 4000 Liège, Belgium

[b] Bulk Superconductivity Group, Engineering Department, University of Cambridge, Cambridge, CB2 1PZ, UK

[*] Corresponding author. Tel.: +32 4 366 2671. E-mail address: M.Philippe@ulg.ac.be

Abstract

Large grain, bulk Y-Ba-Cu-O (YBCO) high temperature superconductors (HTS) have significant potential for use in a variety of practical applications that incorporate powerful quasi-permanent magnets. In the present work, we investigate how the trapped field of such magnets can be improved by combining bulk YBCO with a soft FeNi, ferromagnetic alloy. This involves machining the alloy into components of various shapes, such as cylinders and rings, which are attached subsequently to the top surface of a solid, bulk HTS cylinder. The effect of these modifications on the magnetic hysteresis curve and trapped field of the bulk superconductor at 77 K are then studied using pick-up coil and Hall probe measurements. The experimental data are compared to finite element modelling of the magnetic flux distribution using Campbell's algorithm.

Initially we establish the validity of the technique involving pick-up coils wrapped around the bulk superconductor to obtain its magnetic hysteresis curve in a non-destructive way and highlight the difference between the measured signal and the true magnetization of the sample. We then consider the properties of hybrid ferromagnet/superconductor (F/S) structures. Hall probe measurements, together with the results of the model, establish that flux lines curve outwards through the ferromagnet, which acts, effectively, like a magnetic short circuit. Magnetic hysteresis curves show that the effects of the superconductor and the ferromagnet simply add when the ferromagnet is saturated fully by the applied field. The trapped field of the hybrid structure is always larger than that of the superconductor alone below this saturation level, and especially when the applied field is removed. The results of the study show further that the beneficial effects on the trapped field are enhanced when the ferromagnet covers the entire surface of the superconductor for different ferromagnetic components of various shapes and fixed volume.

Keywords

Bulk superconductor; Magnetic measurement; Trapped field; Ferromagnet

1 Introduction

Bulk superconductors and ferromagnetic materials modify the path of magnetic flux in magnetic circuits in fundamentally different ways, so any combination of these materials often leads to very interesting magnetic behaviour of the composite structure. Superconductors may either repel individual, quantized flux lines completely (i.e. perfect diamagnetism) or, in the case of type-II superconductors containing strong pinning, restrict their movement and act potentially as very strong quasi-permanent magnets. In contrast, due to their high magnetic permeability, ferromagnetic materials tend to channel magnetic flux by providing a low reluctance path. Superconductors can therefore be combined with ferromagnets to modify the distribution of the magnetic flux lines and to improve the superconducting properties of the composite structure. This interplay may arise on (i) a small (sub-micron) scale by the introduction of ferromagnetic particles to the bulk superconducting microstructure [1 – 7], (ii) a millimetre-scale for coated conductors where the use of magnetic substrates and surrounding shields may improve the current distribution [8] and reduce the AC losses [9 – 14], and (iii) a macroscopic scale to improve the performance of various practical applications involving bulk type-II superconductors used as quasi-permanent magnets with a large flux density:volume ratio [15 – 18]. The present study deals precisely with large, bulk Y-Ba-Cu-O (YBCO) on the centimetre scale. The purpose of the investigation is to determine experimentally how the magnetic flux density both inside and outside a solid, cylindrical bulk superconductor is modified when placed in the vicinity of axisymmetric ferromagnetic components of various sizes and shapes, machined out of a well characterized, soft magnetic alloy of high permeability.

At present, large, bulk (RE)BCO high temperature superconductors (HTS), where RE denotes a rare-earth ion, and MgB_2 are the most promising candidates for the development of quasi-permanent magnets that can trap flux densities in excess of 2 T [15 – 18]. These magnets can be used potentially in various engineering applications [19], such as rotating machines [20, 21], magnetic levitation systems [22, 23], magnetic bearings [24, 25], cancer therapy [26] and waste water treatment [27]. Several authors have reported that such applications can be improved by using ferromagnet/superconductor heterostructures. As an example, the flux generated in an iron rotor can be increased by the use of an YBCO frame to screen the flux within the yoke [28]. Hybrid structures can be used to modulate the shape of the magnetic field and/or to increase the magnitude or gradient of the flux density [8, 29 – 33]. Sandwiching a bulk HTS between two soft ferromagnetic yokes can also improve the pulse field magnetization process [34]. Additional applications include, for example, retardation of the magnetic relaxation [35], enhancement the magnetic shielding properties [36 – 38], metamaterials for magnetic cloaking [39] or bulk HTS superconductors containing a regular array of artificial holes filled with a ferromagnetic powder to improve the field trapping properties of the composite sample [40]. In the present work, we use magnetic measurements and numerical modelling to investigate the interaction between a bulk superconductor (S) and a ferromagnet (F) during a *full* magnetic hysteresis cycle. In particular, the hysteresis cycle of the hybrid F/S structure is compared to that of the two materials characterized separately and the influence of the shape and volume of the ferromagnet is determined. In contrast to previous studies, two different techniques that probe both *surface* and *volume* DC magnetic properties are combined on the same large, bulk superconducting sample. The first technique involves placing Hall probes at the centre of the top and bottom surfaces of the superconductor, whereas the second involves pick-up coils wrapped tightly around the body of the superconductor.

Modelling results obtained using both Brandt and finite element methods are used to help understand how the ferromagnetic components modify the magnetic flux density inside and outside the bulk superconductor.

2 Experiment

2.1 Superconducting sample

A solid, cylindrical bulk YBCO superconductor of diameter 16.5 mm and height 6.32 mm, with its *c*-axis parallel to its thickness, was synthesized using conventional top seeded melt growth (TSMG) at the University of Cambridge (UK). The melt-processed, large grain microstructure consists of a superconducting $YBa_2Cu_3O_{7-\delta}$ (Y-123) phase matrix containing discrete Y_2BaCuO_5 (Y-211) inclusions [41, 42]. The top and bottom faces of the as-processed grain were polished prior to characterisation.

2.2 Experimental arrangement for magnetic characterisation

Six sensors were attached to the YBCO sample to enable magnetic characterisation. These consisted of four pick-up coils and two Hall probes, as shown schematically in figure 1. The pick-up coils were made of 80 µm-diameter copper wire wound tightly around the superconductor. The first coil had 53 turns and was wrapped around the entire height of the cylinder in a single layer (i.e. with its principal axis parallel to the thickness of the sample). The three other coils were wrapped around the top, middle and bottom sections of the solid cylinder (as shown in figure 1). The top and bottom coils consisted of 19 turns (one single layer) whereas the middle coil, centred on the median plane of the cylinder, consisted of 44 turns wound in two layers. There was a 1 mm gap between two adjacent coils. The two Hall probes (Arepoc AHP-H3Z, with a 1 mm^2 active area), driven by a current of 1 mA, were placed at the centre of top and bottom surfaces of the cylinder to probe the axial component (i.e. normal to the surface) of the magnetic field. The same arrangement of pick-up coils and Hall probes was used for the ferromagnet/superconductor hybrids, for which the top Hall probe was placed at the top of the hybrid structure. In this case a coil was not wound around the ferromagnet.

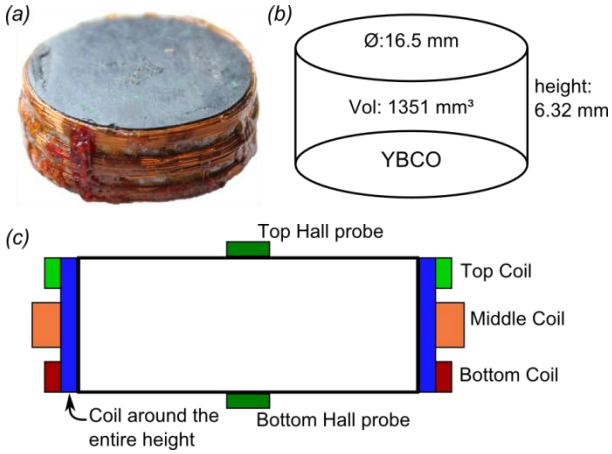

Fig. 1. (a) Photograph of the YBCO sample, (b) dimensions of the YBCO sample and (c) sectional view of the YBCO sample and the six sensors consisting of four coils (wound around the entire height and individually around the bottom, middle and top sections of the YBCO sample) and two Hall probes (centred on the top and bottom surfaces).

The properties of the hybrid structures were measured as a function of temperature and field using a Physical Property Measurement System (PPMS) supplied by Quantum Design. This instrument allows the application of magnetic fields of up to 9 T at a rate of up to 17 mT/s. The instrumented sample was clamped in a closed sample holder to avoid movement due to magnetic forces during the measurement and to enable external interface to the sensors. All measurements in the superconducting state were performed at 77 K, with the calibration of the sensors performed at 100 K (i.e. above the YBCO superconducting transition temperature).

All measurements reported in this investigation involved cooling down the sample in zero field (the so-called zero field cooled, or ZFC, procedure) and then applying a slowly time-varying magnetic field parallel to the *c*-axis of the sample. The field was swept initially up to 3 T and then cycled between 3 T and -3 T using a sweep rate of 15 mT/s. This rate was sufficiently slow to neglect any variation of the applied field between two successive measurements with the different sensors. A time changing magnetic field at a small but finite sweep rate, however, is mandatory for a pick-up coil measurement technique. Each pick-up coil produces a small electromotive force (e.m.f.) proportional to the time variation of the magnetic flux threading the coil via Faraday's law. This induced voltage (typically of the order of a few tens of microvolts for the coils used in this study) was measured and integrated numerically over time to yield a measure of magnetic flux. The resulting flux is divided by the surface of the coil multiplied by the number of turns in order to determine the average magnetic flux density across the bulk superconductor. In this case, the resulting field is equal to the volume average of the z-component of the flux density since all coils were arranged such that their axes of symmetry coincide with that of the sample (the “z”-axis). Each electric signal component of the experiment (the induced e.m.f. across the coils and Hall probe voltages) was measured by a nanovoltmeter (Agilent 34420A), computer controlled using a PC running LabVIEW®.

Great care was taken to measure the voltage offsets twice for each sensor: once before and once after each measurement. Any offset was assumed to have varied linearly during the measurement cycle, and the interpolated linear variation was subtracted from the raw data in the event of the two

offset measurements not being equal. The measured voltages were converted to a magnetic induction based on the calibration at 100 K.

2.3 Ferromagnetic components

The ferromagnetic components were machined from the commercial, soft ferromagnetic alloy *Supra50* [43] (note that this name has nothing to do with superconductivity!). This alloy is composed mainly of iron and nickel (51.5 wt% and 47 wt%, respectively). Its magnetic properties were measured independently using a permeameter, which enabled the intrinsic magnetic hysteresis *B*(*H*) curve of long magnetic rods to be determined (see inset of figure 2). A high permeability soft iron yoke was used in this measurement to close the magnetic circuit and to act as a magnetic short circuit in order to avoid demagnetizing effects. Figure 2 shows the *B*(*H*) hysteresis curve measured for a long rod of *Supra50*. The coercive field is found to be 520 A/m and the saturation magnetization $\mu_0 M_{sat}$ to be around 1.4 T. The maximum differential permeability (i.e. the slope of the hysteresis curve at B = 0) is $\mu'_{max} = (\mathrm{d}B/\mathrm{d}H)_{B=0} = 1.7 \times 10^3 \mu_0$.

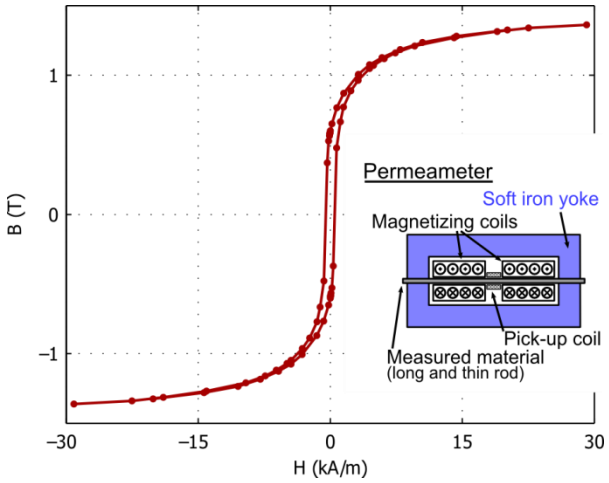

Fig. 2. B(H) hysteresis curve measured for a long rod of Supra50 FeNi alloy. The coercive field is found to be 520 A/m and the saturation magnetization $\mu_0 M_{sat}$ is about 1.4 T. The maximum differential permeability is $1.7 \times 10^3 \mu_0$. The inset shows a schematic sectional view of the permeameter used to perform this measurement.

Four different ferromagnetic components were attached to the top surface of the superconductor using GE 7031 cryogenic varnish to form the ferromagnet/superconductor hybrids, as illustrated in figure 3. All the ferromagnetic components shown in this figure have an external diameter of 16.5 mm, which is the same as that of the bulk, superconducting sample. The experiments were carried out using the following geometries: (*i*) two plain discs of thickness 1.90 mm and 2.90 mm (labelled *C1* and *C4* in figure 3), (*ii*) an inverted cone of height 2.88 mm at the edge and 0.09 mm at the centre (labelled *C2* in figure 3) and (*iii*) a ring (*C3*) of height 2.88 mm and internal diameter 9.52 mm. Significantly, the thin disc, the inverted cone and the ring (i.e. *C1*, *C2* and *C3*) have the same volume (≈ 412 mm^3 within an accuracy of 3%, as summarized in table 1). The volume of the thick disc, however, is ≈ 50% larger (623 mm^3).

DOI: 10.1016/j.physc.2014.04.025

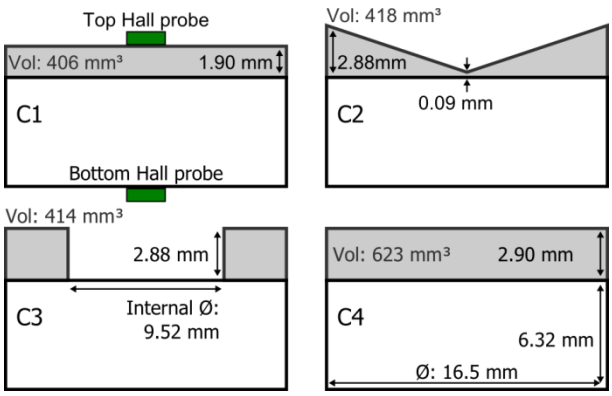

Fig. 3. Cross sections and dimensions of the hybrid ferromagnetic (shaded)/superconductor (white) configurations (F/S hybrids) investigated here. The ferromagnetic components and superconductor each have an external diameter of 16.5 mm. The superconductor has a volume of 1351 mm^3. The position of the Hall probes is shown for configuration *C1*.

3 Modelling

Two different computational models were used; the Brandt method and Campbell's equation solved using a finite element method. These two methods are described briefly as follows.

Initially, we use a numerical model based on the Brandt algorithm [44] to determine the current distribution as a function of the applied field inside the volume of the superconductor only (no ferromagnet). This method is based on the discretization and numerical integration of the Biot–Savart equations. A $J_c(B)$ dependence that follows the Bean-Kim law [45] $J_c(B) = J_{c1}\,(1 + B/B_1)^{-1}$ was assumed in the first instance for the YBCO sample and used to determine the current distribution inside the superconductor for arbitrary values of J_{c1} and B_1. The magnetic induction inside the sample was determined from the modelled current distribution, and its axial component averaged over the whole sample. The resulting hysteresis curve for a full cycle of applied field was compared to the measurements and the sample parameters J_{c1} and B_1 were determined by minimizing the least square error between the computed and measured curves using a trust region algorithm. The average DC magnetization ***M*** defined as the total magnetic moment ***m*** divided by the volume *V* of the sample

$$\boldsymbol{M} = \frac{\boldsymbol{m}}{V} = \frac{1}{V}\int \frac{\boldsymbol{r}\times\boldsymbol{J}}{2}\,\mathrm{d}^3\boldsymbol{r} \qquad (1)$$

was also determined from the current distribution.

Secondly, numerical modelling studies were performed using a modelling framework developed at the University of Cambridge (UK) [46, 47] in order to understand the dynamics of magnetic flux penetration. This modelling framework can simulate various magnetization processes of bulk superconductors by solving Campbell's equation [48] (which describes the force-displacement relation of magnetic flux lines [49, 50] and gives the critical state directly) using the finite element method (FEM) in a commercial software package. The $J_c(B)$ relation of the bulk YBCO superconductor is described by the Kim model, where the parameters J_{c1} and B_1 were determined from magnetic

measurements as discussed in section 4.1.1. On the other hand, the soft ferromagnetic property of the iron-nickel alloy *Supra50* is incorporated by modifying the left hand side of Campbell's equation from $\nabla \times (\nabla \times \boldsymbol{A})$ to $\nabla \times ((\nabla \times \boldsymbol{A})/\mu_r)$, where μ_r is estimated by the function;

$$\mu_r = \mu_{r-max} \text{ for } B_{app} = 0$$

$$\mu_r = 1 + \frac{\text{sgn}(B_{app})\,\mu_0 M_{sat}}{B_{app}}\left[1 - \exp\left(-\frac{\mu_{r-max}\,|B_{app}|}{\mu_0 M_{sat}}\right)\right] \text{ for } B_{app} \neq 0$$

where $\mu_{r-max} = 1.7 \times 10^3$ and $\mu_0 M_{sat} = 1.4$ T. The *B-H* curve deduced from this function agrees reasonably well with the experimental curve shown in figure 2, and it ensures that the slope at $B = 0$ is equal to $1.7 \times 10^3\ \mu_0$. The phenomenon of hysteresis, however, is not taken into account in either model since the coercive field measured is extremely small.

4 Results and discussion

4.1 Measurements on the superconductor only

4.1.1 Magnetic hysteresis loop and magnetization

In this section we focus initially on the volume properties of the bulk superconductor only using the pick-up coil wrapped around the entire thickness of the sample, as described in section 2.2. The voltage appearing across this pick-up coil when the external field is changed is integrated to obtain $\langle B \rangle$, the z-component of the magnetic flux density averaged over the whole sample. Figure 4 shows the measurement results (blue curve with dots) obtained when the applied field is cycled slowly between 3 T and -3 T using a sweep rate of 15 mT/s. In order to obtain a "classical" hysteresis cycle, the applied magnetic field H_{app} multiplied by μ_0 was subtracted from the measured flux density; the experimental data plotted in figure 4 therefore represent $\Delta B = \langle B \rangle - \mu_0 H_{app}$ as a function of $\mu_0 H_{app}$.

Numerical modelling was carried out using the Brandt method as described in section 3 in order to determine the field-dependent critical current of the sample and to emphasize the difference between the measured hysteresis curve and a "true" magnetization curve. A $J_c(B)$ dependence following Bean-Kim law [45] $J_c(B) = J_{c1}\,(1 + B/B_1)^{-1}$ was assumed in the first instance and the values of J_{c1} and B_1 parameters were determined as $J_{c1} = 13.8 \times 10^3$ A/cm^2 and $B_1 = 0.987$ T. The modelled hysteresis curve (red line) is compared to the experimental $\Delta B = \langle B \rangle - \mu_0 H_{app}$ curve in figure 4. It can be seen that the agreement with the measured data is very good. The true DC magnetization curve as defined by equation (1) was then calculated using the previously determined values of J_{c1} and B_1, as indicted by the green line in figure 4. This modelled DC magnetization differs considerably from the measured and modelled ΔB hysteresis curves, with the magnetization being approximately 2.5 times greater than ΔB. Similarly, a ratio of 2.4 is found between the initial slopes of the two modelled curves.

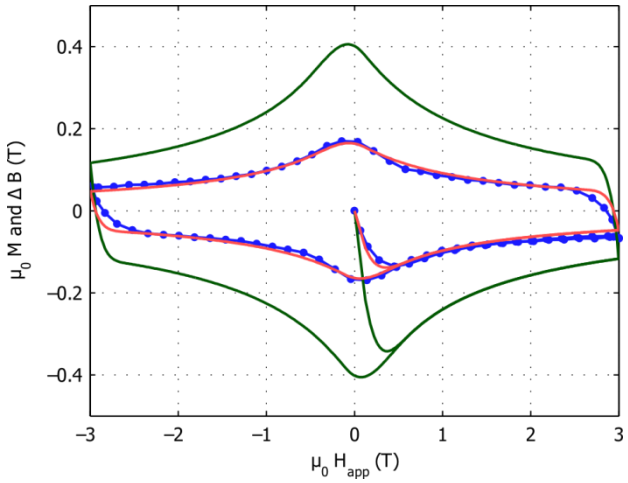

Fig. 4. Comparison between the measured $\Delta B = \langle B \rangle - \mu_0 H_{\mathrm{app}}$ hysteresis curve (blue curve with dots), the computed ΔB hysteresis curve (solid, red curve) and the computed volume DC magnetization M (solid, green curve).

This result underlines the fact that, since the sample is of finite height, the experimental data obtained with the sensing coil do *not* correspond to the DC magnetization of the superconductor [51], although their general appearance is similar. Finite size effects have already been studied on short (low aspect ratio) type-II superconductors using numerical modelling [52, 53], as well as magnetization measurements [54, 55]. However, these studies relate to the magnetization $M(H_{\mathrm{app}})$ rather than the ΔB determined experimentally in the present work. The computed magnetization curve in figure 4 enables the full-penetration field H_{p} to be determined at the point where the first magnetization curve reaches the full hysteresis cycle. In this case, $\mu_0 H_{\mathrm{p}} \approx 0.54\ \mathrm{T}$.

It can be concluded from the above analysis that the experimental system using sensing coils wrapped around the superconductor yields magnetic hysteresis loops that differ quantitatively from, but are closely related to, the DC magnetization. The critical current J_c of the sample can be extracted directly from the magnetization loop [53] but well-established techniques for measuring DC magnetization (such as SQUID and VSM) cannot be applied in the case of a large, single domain (16.5 mm diameter). Commercially available devices generally accommodate samples of much smaller size (typically < 1 cm^3) that require the extraction of small sub-specimens from the parent sample, which is necessarily destructive in nature. The magnetic moment could be measured with the coils positioned at a large distance from the sample [51] but, since single grain bulk superconductors are particularly useful for the fields they generate near their surface, this configuration was measured here. The significant advantage of the experimental method using sensing coils near the sample is that it is suitable for investigating the DC volume magnetic properties and the critical current J_c of large samples. However, the method requires the $J_{\mathrm{c}}(B)$ variation to be assumed and some curve fitting is necessary to determine the value of J_c. Having established its validity, therefore, this experimental method was applied to the superconductor alone and to the superconductor/ferromagnet hybrid structures.

4.1.2 Characterization of the superconductor

Figure 5 (*a*) shows the hysteresis curves of $\Delta B = \langle B \rangle - \mu_0 H_{\mathrm{app}}$ as a function of applied field $\mu_0 H_{\mathrm{app}}$ measured by the four coils wound around the superconductor only: the sensing coil wound around

the entire height of the bulk sample (as shown in figure 4) and the three small coils placed at different locations (top, middle, bottom). The four experimental curves approximate well to each other, which indicates a relatively uniform distribution of the average flux as a function of sample height. The agreement between the data shows also that coils are well suited to measure the average magnetic behaviour of the superconductor, despite the relatively small signals recorded for coils of less than 20 turns.

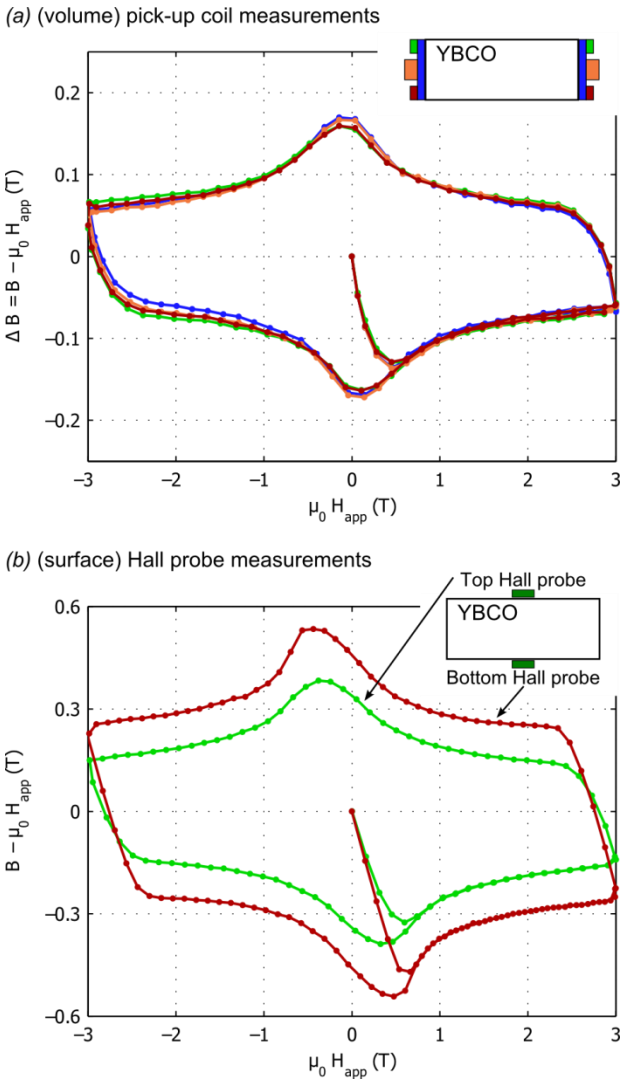

Fig. 5. (*a*) Magnetic hysteresis curves measured with the four coils on the superconductor only. The coil wound around the entire height of the superconductor is shown in blue. The top, middle and bottom coils are shown in green, orange and red, respectively. (*b*) Magnetic hysteresis curves measured by the Hall probes placed against the top (green) and bottom (red) faces of the superconductor.

Figure 5 (*b*) shows the hysteresis curves measured by the Hall probes positioned at the centre of either the top (green) and bottom (red) faces of the bulk superconductor, using the same cycle of applied field employed for the sensing coil measurements. By analogy with the data shown in figure 5 (*a*), we plot $B - \mu_0 H_{\mathrm{app}}$, where *B* now denotes the magnetic flux density at the Hall probe location, as a function of the applied field. Note that the seeded surface of the sample corresponds to the

bottom face of the bulk single domain in the configuration studied here. As can be seen from figure 5 (*b*), the remanent magnetic field measured by the top Hall probe (on the face opposed to the seed) is approximately 25 % lower than that measured by the bottom probe positioned against the seed. Similar discrepancies have been observed in other bulk samples fabricated by the TSMG process [56 – 59], and are related to axial and radial variations of both T_c and J_c within the single domain. In the present case, it is of interest to investigate in more detail the reason why a non-uniform J_c in the bulk sample has a larger effect on the local value of *B* than on the average induction probed by the pick-up coil. First, there might be an effect of a greater J_c in a small volume around the seed. Second, there is also a variation of J_c along the z-axis, which may result on a layer with weaker J_c near the face of the superconductor opposite to the seeding surface. We believe this second effect is predominant here, and can be explained as follows. If we assume an extreme situation in which the weaker J_c layer far from the seed would be a thin non-superconducting layer (approximately 0.5 mm), it can be shown analytically [58, 60] that the central *B* measured by the Hall probe decreases by approximately 25 % compared to the original sample. On the other hand, for the average *B*, the decrease of the remanent flux embraced by the top coil would be only 11 %. This result can be understood qualitatively: the sensing coil still embraces a large part of fully superconducting material whereas the effect on the local *B* is equivalent to inserting a small air-gap between the Hall probe and the sample, leading to a large reduction of the measurement. Significantly, this study indicates that the trapped field measured at the surface of the bulk sample is influenced predominantly by a relatively thin layer of material in the vicinity of the sensor. In addition, Hall probe measurements are sensitive to local variations of J_c, which can be higher near the seed but also lower on the face opposite to the seeding surface. In contrast, sensing coils measure the average magnetic behaviour over the section of the superconductor they surround, and are influenced much less by non-homogeneities in the bulk sample, as evidenced by the results in figure 5 (*a*).

One advantage of probing magnetic properties with the Hall sensors is that magnetic relaxation measurements can be performed easily. The critical exponent *n* can be determined [56] assuming that the remanent magnetization of the superconductor decreases with time as a power law relationship $B \propto (1 + t/t_0)^{1/(1-n)}$, where t_0 is the time before the beginning of the magnetic relaxation [61]. For the case of the bulk superconductor studied in this work, the fit of the power law to the measurement over two days of the remanent magnetization decay gives a critical exponent *n* = 45 for $t \gg t_0$.

4.2 Ferromagnet/Superconductor hybrid structures

We now turn to the magnetic behaviour of ferromagnet/superconductor (F/S) hybrid structures and focus initially on a ferromagnetic disc (of thickness 1.90 mm) placed on the top of the superconductor. This corresponds to the structure *C1*, shown in figure 3. The modelling results are obtained by solving Campbell's equation as described in section 3. This method allows the repartition of the contour lines of the vector potential *A* to be determined easily. For axisymmetric geometries, the contour lines of *A* give a reasonable approximation of the flux lines of *B*, as described in [44].

4.2.1 Flux distribution

Figure 6 shows the modelled repartition of the contour lines of the vector potential *A* when an external magnetic field of $\mu_0 H_{app}$ = 0.3 T is applied to (*a*) the superconductor only and (*b*) the hybrid F/S structure *C1*. This value of applied field corresponds to approximately half the full-penetration

field of the superconductor (see section 4.1.1). Results for the superconductor alone (figure 6 (*a*)) show the expected shape of contour lines in this configuration [44]. When the ferromagnetic disk is added to the superconductor (figure 6 (*b*)), the contour lines of *A* are concentrated inside the ferromagnet and undergo a strong change of direction at the edges of the ferromagnet: the lines are nearly perpendicular to the interface on the air and superconductor sides. These contours indicate that the magnetic flux distribution in the bottom part of the superconductor remains relatively unaffected, whereas the flux penetrates the superconductor less in the vicinity of the ferromagnet. However, the density of *A* lines in the air above the ferromagnet (figure 6(b)) is higher than that above the superconductor alone (figure 6(a)).

Figure 7 shows the path followed by the contour lines of *A* in the fully magnetized remanent state (trapped field) for (*a*) the superconductor only configuration and (*b*) the hybrid F/S structure *C1*. Compared to figure 7(a), the results shown in figure 7(*b*) indicate that the contour lines are strongly concentrated inside the ferromagnet. The contours are almost perpendicular to the ferromagnet interface in the low permeability domain (air or superconductor). The concentration of *A* lines is much smaller than the case without ferromagnet above the top face of the F/S assembly.

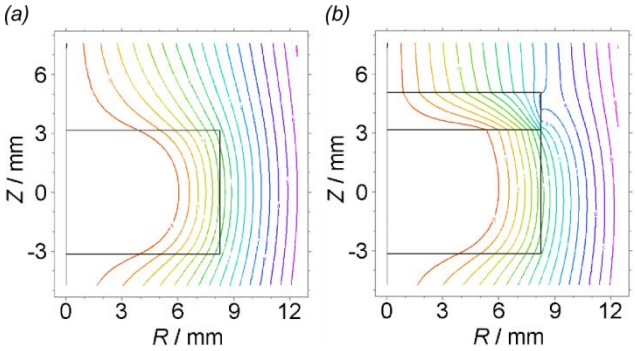

Fig. 6. Repartition of the contour lines of the vector potential *A* for an external applied field of $\mu_0 H_{app}$ = 0.3 T inside (*a*) the superconductor only and (*b*) the hybrid ferromagnet/superconductor (F/S) structure *C1*. These results are obtained by solving Campbell's equation as described in section 3.

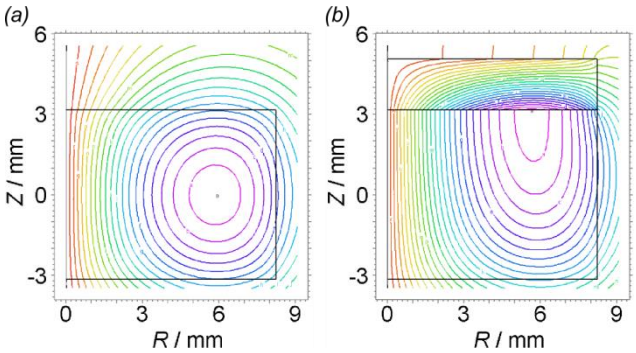

Fig. 7. (*a*) Contour lines of the vector potential *A* in the fully magnetized remanent state for the superconductor described in section 2.1. These results are obtained by solving Campbell's equation as described in section 3. (*b*) Same contour lines for the hybrid ferromagnet/superconductor (F/S) structure *C1*.

These results emphasize that the high permeability ferromagnet acts as a magnetic short-circuit for magnetic flux density since it creates a low reluctance path. When the assembly is subjected to an external magnetic field (figure 6), the penetration of the magnetic flux inside the superconductor is delayed in the vicinity of the ferromagnet. The zone above the ferromagnet in the trapped field configuration (figure7) is shielded from the flux trapped inside the superconductor. Moreover, the flux lines that were closed through the superconductor are now closed through the ferromagnet, which leads to a decrease of the curvature of the return flux lines inside the superconductor. In addition, the flux lines are perpendicular to the median plane of the superconductor in the absence of the ferromagnet whereas they are perpendicular to the ferromagnet/superconductor interface in presence of the ferromagnet. Therefore, adding the ferromagnet can be assimilated to doubling the height of the superconductor as expected in the limit case of a semi-infinite ferromagnet of infinite permeability where the effect of the ferromagnet can be replaced by an image of the superconductor [30, 62, 63]. The doubled height corresponds to an increase of the effective aspect ratio of the sample and a reduction of the edge effect of a finite length sample.

4.2.2 Hysteresis loops

Figure 8 shows the hysteresis loop measurements obtained for the hybrid *C1* F/S configuration modelled in the previous section (1.90 mm thick ferromagnetic disc above the superconductor).

Figure 8 (*a*) compares the $\Delta B = \langle B \rangle - \mu_0 H_{\mathrm{app}}$ magnetic hysteresis loops recorded by the four pick-up coils. The hysteresis loop measured with the coil wound around the superconductor only is also shown for comparison (light blue dots). The hysteresis loops of the F/S hybrid structure show a combination of diamagnetic (negative slope at the origin) and ferromagnetic behaviour (the average *B* exceeds $\mu_0 H_{\mathrm{app}}$ at medium and high positive applied fields). The behaviour at high applied field (typically for $\mu_0 H_{\mathrm{app}} > 1$ T) highlights some differences between the four coils: for a given applied field, the magnetic induction measured by the top coil (green triangles) in the vicinity of the ferromagnet is higher than that measured by the bottom coil (red triangles), located more distant from the ferromagnet. The coils wound around the middle (orange squares) and entire height (navy blue circles) of the sample show an intermediate behaviour, except above 1.5 T where the middle section exhibits the lowest ΔB. Compared to the superconductor alone, the remanent induction (measured at $\mu_0 H_{\mathrm{app}} = 0$) is increased by 8.8%, 15% and 29% for the bottom, middle and top sections, respectively. The magnetic flux probed by the coil wound around the entire height of the superconductor shows an increase of 16% of the remanent magnetic induction.

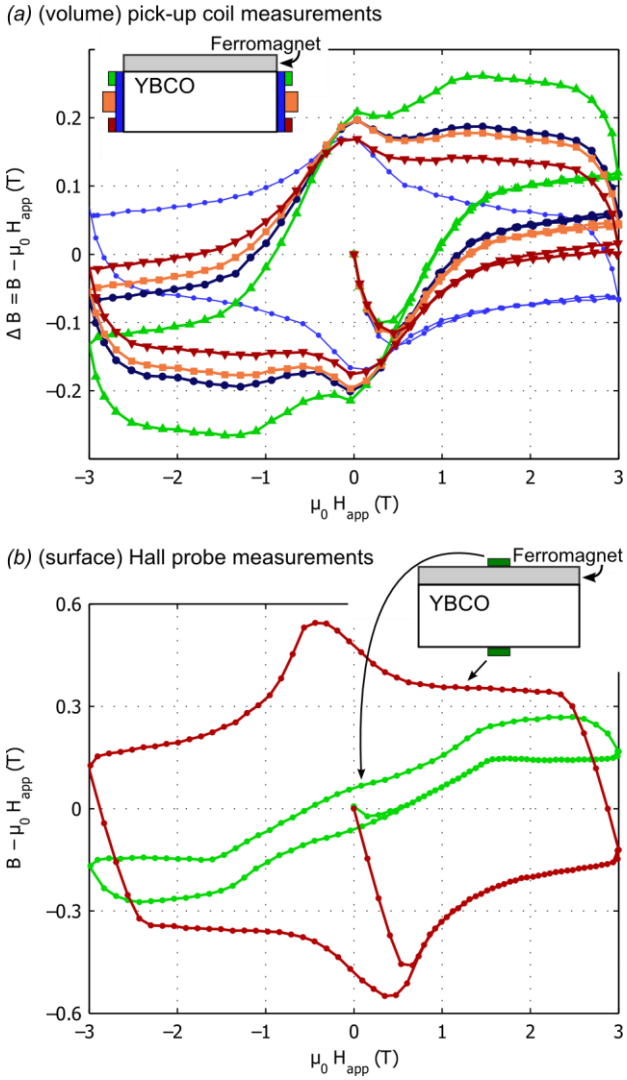

Fig. 8. (*a*) Magnetic hysteresis curves measured with the four coils on the *C1* ferromagnet/superconductor configuration. The navy blue circles represent the data for the coil wound around the entire sample height. The green triangles, orange squares and red triangles are for the top, middle and bottom coils, respectively (i.e. the colours of the coils refer to those shown schematically in the inset). The curve for the coil wound around the entire height of the superconductor only is shown for comparison (blue dots). (*b*) Magnetic hysteresis curves measured by the Hall probes placed against the top (green) and bottom (red) faces of the bulk superconductor.

The hysteresis curves shown in figure 8 (*a*) provide experimental evidence of a strongly non-uniform distribution of the magnetic induction through the thickness of the superconductor. In addition, when the external field is modified, the evolution of ΔB depends on the proximity of each section within the sample to the ferromagnet. The variations of the applied field have clearly more effect on the magnetic induction in the sections near the ferromagnet. At zero applied field, the fact that the average remanent induction B_z probed by the pick-up coil around the superconductor is larger in the presence of the ferromagnet, is entirely consistent with the modelling result of figure 7: the

measured B_z increases since the flux lines in the superconductor are perpendicular to the F/S interface and are then driven toward the outside of the superconductor by the ferromagnet.

Figure 8 (*b*) shows surface measurements by the Hall probes on the hybrid F/S structure for the configuration *C1*. The top probe is above the ferromagnet and the bottom probe is against the superconductor (see inset). As is the case in the previous section, the superconductor is always oriented with the seed on the bottom of the configuration. The shape of the magnetic hysteresis curve is roughly similar to that of the superconductor only for the Hall probe located at the bottom (red curve), but appears somewhat tilted anticlockwise with remanent magnetic induction increased slightly by 4%. The full penetration field does not differ significantly from that measured for the superconductor alone. The shape of the hysteresis curve measured by the Hall probe positioned on the top of the ferromagnetic disc (green curve), however, is modified strongly, and appears more like the hysteresis curve of a ferromagnetic material than that of a diamagnetic material. The initial slope of the first magnetization curve is still negative but above ≈ 0.5 T, the quantity $\langle B \rangle - \mu_0 H_{\mathrm{app}}$ becomes positive. Significantly, the remanent magnetic induction is 83% smaller than for the configuration without the ferromagnet.

The above measurements are consistent with the modelling results discussed in the previous section. There is little change of the trapped field by the ferromagnet on the bottom face, as sensed by the Hall probe. The results of figure 8 support the observation in figure 6 and 7 that flux lines are concentrated into the low reluctance ferromagnetic material on the top (ferromagnet) side. Indeed, the flux lines are driven toward the top Hall probe during initial magnetization of the sample (i.e. during the field cycle $0 \rightarrow H_{\mathrm{max}}$), whereas this probe is shielded from the trapped flux by the ferromagnet in the remanent state. Such a magnetic shielding effect leads to a marked reduction of the magnetic field in the air on the ferromagnet side. This observation, although at first sight surprising, yields the following practical conclusion: if the superconducting permanent magnet is used to produce magnetic field in the air, a ferromagnet should not be added on the side where the magnetic field is produced. However, if the relevant quantity is the average flux density trapped in the volume of the superconductor, a ferromagnet is helpful in increasing the trapped flux since its effect is similar to doubling the height of the superconductor, and therefore the aspect ratio of the configuration.

In addition to the previous observations, it is of interest to compare the average flux density of the *C1* hybrid structure – as measured by the coil wound around the entire height – to that measured (*i*) for the superconductor only and (*ii*) for this hybrid structure *C1* when the superconductor is in an unmagnetized state (i.e. above its critical transition temperature). Figure 9(*a*) shows the hysteresis curve measured at 77 K using the coil wound around the entire sample thickness for the superconductor only. Figure 9(*b*) shows the hysteresis curve of the ferromagnet measured using the same coil arrangement for the bulk sample (there are no turns around the ferromagnet) measured at 100 K. Figure 9(*c*) compares the data resulting from the simple numerical addition of the two previous measured curves (red data points) and the true experimental data for the hybrid structure at 77 K (blue data points). Similar results were obtained in the four configurations (*C1* to *C4*) for the hysteresis measurements of the bottom Hall probe and the coil over the entire height, as well as in configuration *C1* with the bottom, middle and top coils. Figure 10 shows the modelled hysteresis

curves corresponding to those of figure 9 (*c*), obtained by solving the Campbell's equation as described in section 3.

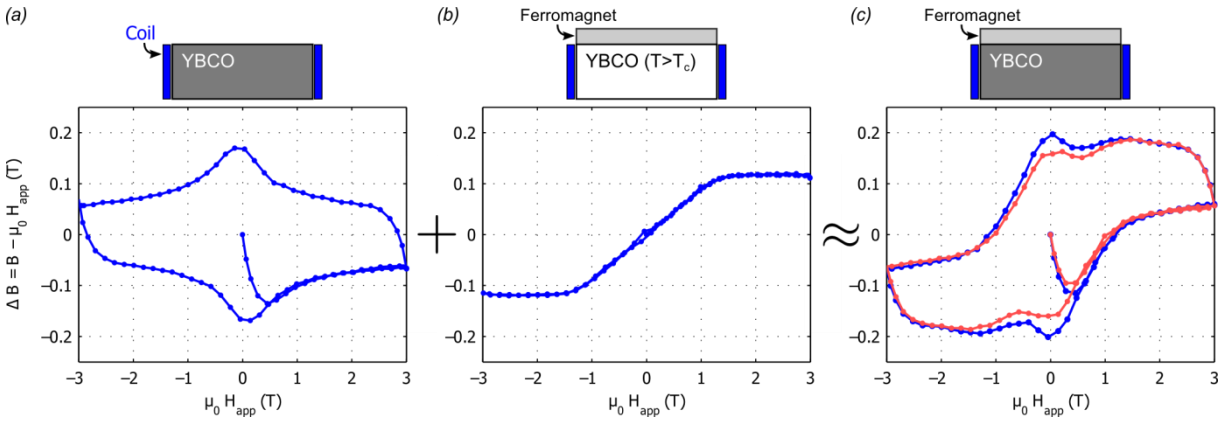

Fig. 9. Magnetic hysteresis loops measured with the coil wound around the entire height of the superconductor for (*a*) the superconductor only at 77 K, (*b*) the small ferromagnetic disc only at 100 K ($T > T_c$), (*c*) the hybrid structure involving this small disc at 77 K (blue). The red curve represents the addition of loops (*a*) and (*b*). The insets show a sectional view of each configuration.

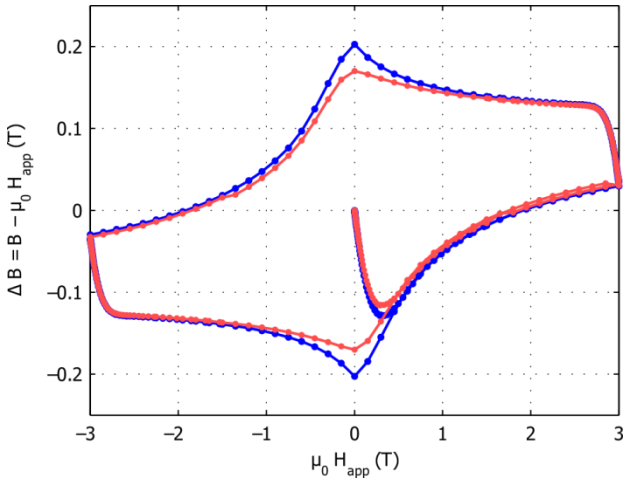

Fig. 10. Modelled magnetic hysteresis loops obtained by solving the Campbell's equation for the hybrid structure *C1* (blue). The red curve was computed in the same way as the red curve in figure 9 (*c*).

Clearly, the hysteresis data in figure 9 show that the magnetic flux density measured for the hybrid structure approximates very well to the simple superposition (i.e. addition) of the individual hysteresis curves of the ferromagnet and the superconductor. The curves are in a particularly good agreement for applied magnetic fields exceeding the apparent saturation field of the ferromagnetic component ($\mu_0 H_{\mathrm{app}} \approx 1.3\ \mathrm{T}$). It is worth noting that this apparent saturation field may differ substantially from the intrinsic saturation field of the ferromagnet for two reasons: (*i*) the measuring coil probing the magnetic flux (figure 9 (*b*)) is wound *below* the ferromagnet and (*ii*) the low aspect ratio of the ferromagnetic disk gives rise to a large demagnetizing field. When the ferromagnet is saturated totally by the external field, the flux densities due to the ferromagnet and the superconductor simply add together. Below this saturation limit, however, the non-uniformity of the

DOI: 10.1016/j.physc.2014.04.025

field may lead to saturation of only some regions of the ferromagnet, and the attraction of the return flux lines to the non-saturated regions of the ferromagnet explains the increase of the remanent induction, as described previously. Remarkably, the results obtained by numerical modelling (figure 10) display the two main qualitative features observed in the experiment, i.e. the additive behaviour at large fields and the larger trapped field for the hybrid configuration compared to the simple numerical addition. The quantitative agreement between figure 9 (*c*) and 10 is also excellent and underlines the suitability of the modelling method to describe the F/S assemblies as well as the importance of using accurate data on the two materials (ferromagnet and superconductor) through preliminary experimental characterization.

4.2.3 Influence of the ferromagnet shape and size

In this final section we examine how the shape and size of the ferromagnet placed against the superconductor modify the previous results obtained with the thin ferromagnetic disc. Figure 11 shows the hysteresis curves measured with the coil wound around the entire height of the superconductor for the different F/S hybrid structures described in figure 3. The curve for the superconductor only is also shown (blue dots) for comparison. Table 1 summarizes the respective volumes of the ferromagnetic components and the corresponding remanent inductions of the curves in figure 11. Each hysteresis loop exhibits a combination of diamagnetic and ferromagnetic behaviour, as is the case for the configuration with the thin disc (*C1*). The slope at the origin of the axes remains unchanged by the presence of the ferromagnet, although its presence leads to a change of sign of ΔB as the applied field increases. It can be seen further that the maximum of the curve appearing around $H \approx 0$ (strictly speaking, at a slightly negative applied field for the superconductor only) is shifted to the right and appears now for a positive applied field for all configurations of the hybrid structure. The remanent induction (measured at zero applied field) is also increased by the presence of the ferromagnetic component, as listed in table 1.

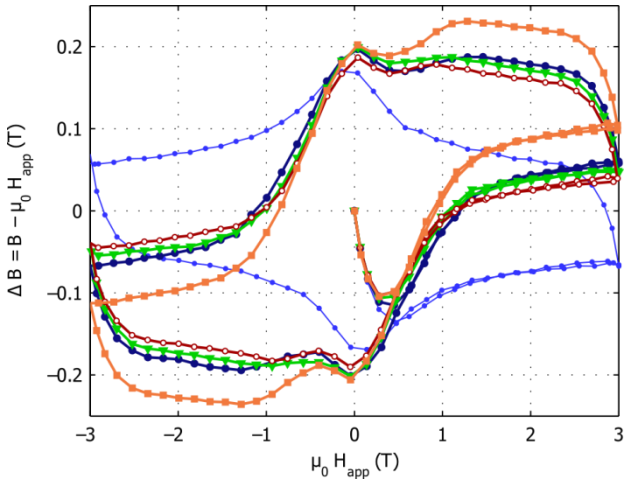

Fig. 11. Magnetic hysteresis loops measured with the coil wound around the entire height of the superconductor for the superconductor only (blue dots) and the four F/S configurations shown in figure 3: *C1* (1.90 mm disc, navy blue circles), *C2* (inverted cone, green triangles), *C3* (ring, red empty circles) and *C4* (2.90 mm disc, orange squares).

Table 1. Evolution of the average remanent induction for the configurations C1 to C4 (see figure 3) compared with the volume of the ferromagnet (F). The superconductor (S) has a volume of 1351 mm^3.

F/S hybrid	Volume: S+F (mm^3)	B_{rem} (T)	Increase of B_{rem} (%)
S only	1351	0.168	--
C1	1351+406	0.196	16
C2	1351+418	0.196	16
C3	1351+414	0.189	12
C4	1351+623	0.198	18

The comparison of the four hybrid configurations can be made (*i*) with two components of the same shape (disk) and different volumes (*C1* vs. *C4*) or (*ii*) with three ferromagnetic components of (almost) the same volume but with different shapes (*C1* to *C3*). This comparison is based here on the measurements with the coil wound around the entire height of the superconductor and similar results were obtained for the three other coils (top, middle, and bottom). The Hall probes do not lead to significant conclusions about the effect of the shape of the ferromagnet since the top probe is partially shielded by the ferromagnet and the bottom one is too far to detect a significant effect of this ferromagnet.

The quantitative effects described above increase in magnitude as the volume of the ferromagnet increases. The increase of remanent induction is also higher for a larger volume, although this increase varies more slowly than in direct proportion. More precisely, the 2.90 mm thick disc, with a 53% larger volume than the 1.90 mm disc, leads only to a 10% larger increase of the remanent induction (from 16% to 18%).

The shape effect can be appreciated by comparing the results for the small disc (*C1*), the inverted cone (*C2*) and the ring (*C3*). As can be seen from figure 11, the ring produces the smallest increase of the remanent induction (12%), while the disc and the inverted cone both lead to an increase of 16%. Such behaviour can be understood qualitatively as follows. Whereas they both have the same volume, the ring is thicker than the disc (2.88 mm compared to 1.90 mm) and does not cover the centre of the superconductor. The most distant part of the ferromagnet has a small effect on the induction inside the superconductor, as observed from the measurements on the discs. These observations suggest that the presence of ferromagnetic material *against the whole surface* of the superconductor is important. It is therefore preferable to locate the ferromagnet as close as possible to the superconductor. In addition, a thinner ferromagnetic disk than those investigated here could yield a better effect:volume ratio. Hence, the effect:volume ratio of the ferromagnet could be maximized for a specific ferromagnet volume. The experimental results show further that the inverted cone geometry and the 1.90 mm thick disc produce a similar increase of the remanent induction in the hybrid structure, despite the inverted cone being slightly larger (3.2%) than the disc. The present measurements provide only a limited explanation of this observation, but it could be due to the uncertainty of the measurement, a consequence of different return paths of the magnetic flux

or the fact that the ferromagnet is subjected to a highly non-uniform magnetic field and may contain saturated and non-saturated regions.

The position of the maximum magnetization for negative applied fields in the case of a pure superconductor has been associated with a minimization of the magnetic flux inside the material (i.e. consisting of the sum of the applied field and the trapped field), which leads to an increase in the field dependent critical current [53]. The observed shift of the position of these maxima to positive applied fields for the hybrid F/S structure suggests that the increase of the remanent field is related to the closing of the return flux lines outside of the superconductor. As discussed above, the ferromagnet acts as a magnetic short-circuit and channels the return path of the magnetic flux outside the body of the superconductor.

5 Conclusion

The magnetic properties of hybrid structures made of a soft ferromagnet attached to a bulk, large grain superconductor (F/S) were characterized both experimentally and numerically. *Surface* (Hall probe) measurements were compared to *volume* measurements carried out using four coils wound around the entire height and around the top, middle and bottom sections of the superconductor. Numerical modelling using the Brandt method and Campbell's equation were performed to draw important conclusions about the magnetic flux distribution in and around the assemblies.

In the first series of experiments and modelling, we focused on the experimental technique that was used for obtaining volume magnetic properties on large bulk samples, with or without ferromagnet. We have shown that sensing coils wrapped around the superconductor enable "quasi"' DC (i.e. low sweep rate) magnetic hysteresis loops to be measured on large, bulk samples. We have pointed out the quantitative differences between the as-measured hysteresis loop and the "true" DC magnetization loop predicted numerically. Despite these differences, this experimental technique is helpful for characterising, in a non-destructive way, the *volume* magnetic properties, as the field-dependent critical current, of whole large superconducting samples whose dimensions exceeds the maximum size of classical DC magnetometers.

Hybrid F/S structures were also studied as part of this investigation. Surface measurements using Hall probes showed that the probe placed against the ferromagnet is screened by the ferromagnet, whereas that placed against the opposite face of the sample is too distant to detect significant modifications of the magnetic induction caused by this component. The fact that the ferromagnet acts as a shield by concentrating and deflecting the magnetic flux lines produced by the superconducting magnet emphasizes that such a ferromagnetic element should not be placed in a zone where a large magnetic field in the air is desired. As far as the volume magnetic flux through the superconductor is concerned, however, the effect of the ferromagnet is beneficial to the trapped flux. This effect was studied using sensing coils wound around the superconductor. The corresponding hysteresis loops show a combination of diamagnetic and ferromagnetic behaviour, with the ferromagnet having a larger effect on the sections of the superconductor in closer proximity to its position. Measurements using the coil wound around the entire sample give insight on how the two materials interact with one another. An important point is that the presence of the ferromagnet increases the remanent induction inside the superconductor in all the configurations studied in this

investigation. This behaviour can be understood by considering the return path of the magnetic flux in the ferromagnet, which decreases the curvature of the flux lines within its interior. It is found by comparing ferromagnetic disks of different volumes that a larger ferromagnet has a more significant effect on the whole hysteresis loop of the superconductor, but this effect varies less than proportionally to the increase in the ferromagnet volume. The beneficial effects on the remanent induction are enhanced by comparison of various ferromagnet shapes with the same volume when the ferromagnet covers the entire surface of the superconductor.

Finally, the relation of the hysteresis cycle of the hybrid F/S structure to that of its two constituent materials characterized separately has been investigated experimentally. The results are in excellent agreement with the predictions of finite element modelling. The hysteresis effects of the superconductor and the ferromagnet simply superimpose at high applied field (i.e. exceeding the apparent saturation of the ferromagnet). Remarkably, this behaviour is observed above the ferromagnetic saturation limit for all the configurations studied in this investigation. Below this level of applied field, the ferromagnet probably contains saturated and non-saturated regions. It seems that such simple "additive" behaviour can be used effectively as a "rule of thumb" for predicting the magnetic behaviour of larger or more complex hybrid structures involving ferromagnets and bulk superconductors.

Acknowledgements

The authors would like to thank Professor A M Campbell for his insight and comments. This work is part of an *Action de Recherches Concertées* grant from the Ministry of Higher Education through the Research Council of the University of Liege (ARC 11/16-03).

References

[1] A. Y. Aladyshkin, A. V. Silhanek, W. Gillijns, V. V. Moshchalkov, Nucleation of superconductivity and vortex matter in superconductor-ferromagnet hybrids, Supercond. Sci. Technol. 22 (2009) 053001.

[2] V. Vlasko-Vlasov, A. Buzdin, A. Melnikov, U. Welp, D. Rosenmann, L. Uspenskaya, V. Fratello, W. Kwok, Domain structure and magnetic pinning in ferromagnetic/superconducting hybrids, Phys. Rev. B 85 (2012) 064505.

[3] K. Xu, K. Tsuzuki, S. Hara, D. Zhou, Y. Zhang, M. Murakami, D. Nishio-Hamane, M. Izumi, Microstructural and superconducting properties in single-domain Gd–Ba–Cu–O bulk superconductors with *in situ* formed Fe_3O_4 ferrimagnetic particles, Supercond. Sci. Technol. 24 (2011) 085001.

[4] A. Palau, H. Parvaneh, N. A. Stelmashenko, H. Wang, J. L. Macmanus-Driscoll, M. G. Blamire, Hysteretic vortex pinning in superconductor-ferromagnet nanocomposites, Phys. Rev. Lett. 98 (2007) 117003.

[5] N. Pompeo, K. Torokhtii, C. Meneghini, S. Mobilio, R. Loria, C. Cirillo, E. A. Ilyina, C. Attanasio, S. Sarti, E. Silva, Superconducting and structural properties of Nb/PdNi/Nb trilayers, J. Supercond. Novel Magn. 26 (2013) 1939 – 1943.

[6] D. Stamopoulos, E. Aristomenopoulou, E. Manios, D. Niarchos, The superconducting magnetoresistance effect in $Ni_{80}Fe_{20}$–Nb–$Ni_{80}Fe_{20}$ and Co–Nb–Co trilayers: Requisites for tailoring its magnitude, J. Supercond. Novel Magn. 26 (2013) 1931–1938.

[7] V. A. Kashurnikov, A. N. Maksimova, I. A. Rudnev, A. P. Sotnikova, Nonlinear interaction of a ferromagnet with a high-temperature superconductor, J. Exp. Theor. Phys. 116 (2013) 476–485.

[8] Y. A. Genenko, H. Rauh, A. Snezhko, Novel design of a smart magnet/superconductor heterostructure, Physica C 372-376, Part 3 (2002) 1389 – 1393.

[9] M. D. Sumption, E. Lee, E. W. Collings, X. L. Wang, S. X. Dou, Suppression of ac (hysteretic) loss by magnetic shielding of MgB_2/Fe superconductors: The pseudo-Meissner effect, AIP Conf. Proc. 614 (2002) 824–831.

[10] F. Gömöry, M. Vojenciak, E. Pardo, M. Solovyov, J. Šouc, AC losses in coated conductors, Supercond. Sci. Technol. 23 (2010) 034012.

[11] M. D. Ainslie, T. J. Flack, A. M. Campbell, Calculating transport AC losses in stacks of high temperature superconductor coated conductors with magnetic substrates using FEM, Physica C 472 (2012) 50–56.

[12] M. D. Ainslie, W. Yuan, T. J. Flack, Numerical analysis of AC loss reduction in HTS superconducting coils using magnetic materials to divert flux, IEEE Trans. Appl. Supercond. 23 (2013) 4700104.

[13] P. Krüger, F. Grilli, M. Vojenciak, V. M. R. Žermeño, E. Demencik, S. Farinon, Superconductor/ferromagnet heterostructures exhibit potential for significant reduction of hysteretic losses, Appl. Phys. Lett. 102 (2013) 202601.

[14] Y. A. Genenko, Magnetic shielding for improvement of superconductor performance, Phys. Status Solidi A 189 (2002) 469–473.

[15] M. Tomita, M. Murakami, High-temperature superconductor bulk magnets that can trap magnetic fields of over 17 tesla at 29 K, Nature 421 (2003) 517–520.

[16] S. Nariki, N. Sakai, M. Murakami, Melt-processed Gd–Ba–Cu–O superconductor with trapped field of 3 T at 77 K, Supercond. Sci. Technol. 18 (2005) S126–S130.

[17] J. H. Durrell, C. E. J. Dancer, A. Dennis, Y. Shi, Z. Xu, A. M. Campbell, N. Hari Babu, R. I. Todd, C. R. M. Grovenor, D. A. Cardwell, A trapped field of 3 T in bulk MgB_2 fabricated by uniaxial hot pressing, Supercond. Sci. Technol. 25 (2012) 112002.

[18] H. Teshima, M. Morita, T. Arayashiki, T. Naito, H. Fujishiro, 10 T class trapped field properties of a large Gd–Ba–Cu–O bulk superconductor, Physics Procedia 45 (2013) 61–64.

[19] B. Li, D. Zhou, K. Xu, S. Hara, K. Tsuzuki, M. Miki, B. Felder, Z. Deng, M. Izumi, Materials process and applications of single grain (RE)–Ba–Cu–O bulk high-temperature superconductors, Physica C 482 (2012) 50 – 57.

[20] X. Granados, M. Torner, T. Puig, X. Obradors, Magnetization of ferromagnetic-SC heterostructures for trapped field low power motors, IEEE Trans. Appl. Supercond. 17 (2007) 1629–1632.

[21] D. Zhou, M. Izumi, M. Miki, B. Felder, T. Ida, M. Kitano, An overview of rotating machine systems with high-temperature bulk superconductors, Supercond. Sci. Technol. 25 (2012) 103001.

[22] S. B. Kim, T. Ikegami, J. Matsunaga, Y. Fujii, H. Onodera, The levitation characteristics of the magnetic substances using trapped HTS bulk annuli with various magnetic field distributions, Physica C 494 (2013) 270 – 275.

[23] I. Sakai, T. Higuchi, Dynamic properties of magnetic levitation system using high-temperature superconductors, IEEE Trans. Appl. Supercond. 21 (2011) 1515–1518.

[24] T. A. Coombs, A. M. Campbell, I. Ganney, W. Lo, T. Twardowski, B. Dawson, Superconducting bearings in flywheels, Mater. Sci. Eng. B 53 (1998) 225–228.

[25] F. N. Werfel, U. Floegel-Delor, R. Rothfeld, T. Riedel, B. Goebel, D. Wippich, P. Schirrmeister, Superconductor bearings, flywheels and transportation, Supercond. Sci. Technol. 25 (2012) 014007.

[26] K. Nakagawa, Y. Ohaku, J. Tamada, F. Mishima, Y. Akiyama, M. K. Osako, H. Nakagami, S. Nishijima, Study on magnetic gene transfer using HTS bulk magnet, Physica C 494 (2013) 262 – 264.

[27] T. Oka, H. Fukazawa, S. Fukui, J. Ogawa, T. Sato, M. Ooizumi, M. Tsujimura, K. Yokoyama, Collection of Ni-bearing material from electroless plating waste by magnetic separation with HTS bulk magnet, Physica C 496 (2014) 58 – 62.

[28] X. Granados, E. Bartolomé, X. Obradors, M. Tornes, L. Rodrigues, W. Gawalek, M. McCulloch, D. Dew Hughes, A. Campbell, T. Coombs, M. Ausloos, R. Cloots, Iron-YBCO heterostructures and their application for trapped field superconducting motor, J. Phys.: Conf. Ser. 43 (2006) 788–791.

[29] S. Kim, T. Nakano, R. Takano, S.-Y. Hahn, Study on trapped field characteristics of HTS bulk annuli with iron rings for ferromagnetic shimming of a compact NMR magnet, IEEE Trans. Appl. Supercond. 19 (2009) 2273–2276.

[30] N. Del-Valle, S. Agramunt-Puig, C. Navau, A. Sanchez, Shaping magnetic fields with soft ferromagnets: Application to levitation of superconductors, J. Appl. Phys. 111 (2012) 013921.

[31] H. Fujishiro, D. Furuta, K. Yaegashi, T. Naito, N. Yoshimoto, Large and spatial magnetic field modulation using superconducting bulk magnet and silicon steel, Physica C 470 (2010) 1856–1859.

[32] M. Ghodsi, T. Ueno, H. Teshima, H. Hirano, T. Higuchi, The characteristics of trapped magnetic flux inside bulk HTS in the Mixed-μ levitation system, Physica C 445-448 (2006) 343 – 346.

[33] G. Ma, J. Wang, S. Wang, M. Liu, H. Jing, Y. Lu, Q. Lin, A novel propulsion method for high-Tc superconducting maglev vehicle, Physica C 468 (2008) 7 – 11.

[34] H. Ikuta, H. Ishihara, Y. Yanagi, Y. Itoh, U. Mizutani, Extracting the utmost from the high performance of Sm–Ba–Cu–O bulk superconductors by pulse field magnetization, Supercond. Sci. Technol. 15 (2002) 606–612.

[35] B. M. Smolyak, G. V. Ermakov, M. S. Zakharov, Retardation of the magnetic relaxation in high-temperature superconductors near a ferromagnet, J. Supercond. Novel Magn. 24 (2011) 325–329.

[36] J.-F. Fagnard, M. Dirickx, M. Ausloos, G. Lousberg, B. Vanderheyden, P. Vanderbemden, Magnetic shielding properties of high-Tc superconducting hollow cylinders: model combining experimental data for axial and transverse magnetic field configurations, Supercond. Sci. Technol. 22 (2009) 105002.

[37] G. P. Lousberg, J.-F. Fagnard, M. Ausloos, P. Vanderbemden, B. Vanderheyden, Numerical study of the shielding properties of macroscopic hybrid ferromagnetic/superconductor hollow cylinders, IEEE Trans. Appl. Supercond. 20 (2010) 33–41.

[38] L. Gozzelino, R. Gerbaldo, G. Ghigo, F. Laviano, A. Agostino, E. Bonometti, M. Chiampi, A. Manzin, L. Zilberti, Magnetic shielding properties of MgB_2Fe superimposed systems, J. Supercond. Novel Magn. 26 (2013) 1513–1516.

[39] J. Prat-Camps, A. Sanchez, C. Navau, Superconductor-ferromagnetic metamaterials for magnetic cloaking and concentration, Supercond. Sci. Technol. 26 (2013) 074001.

[40] G. P. Lousberg, J.-F. Fagnard, X. Chaud, M. Ausloos, P. Vanderbemden, B. Vanderheyden, Magnetic properties of drilled bulk high-temperature superconductors filled with a ferromagnetic powder, Supercond. Sci. Technol. 24 (2011) 035008.

[41] N. Hari Babu, M. Kambara, Y.-H. Shi, D. A. Cardwell, C. D. Tarrant, K. R. Schneider, Processing and microstructure of single grain, uranium-doped Y–Ba–Cu–O superconductor, Supercond. Sci. Technol. 15 (2002) 104–110.

[42] N. Hari Babu, K. Iida, Y. Shi, D. A. Cardwell, Processing of high performance (LRE)–Ba–Cu–O large, single-grain bulk superconductors in air, Physica C 445–448 (2006) 286–290.

[43] Aperam Alloys Imphy, http://www.aperam.com/alloys-imphy/.

[44] E. H. Brandt, Superconductor disks and cylinders in an axial magnetic field. I. Flux penetration and magnetization curves, Phys. Rev. B 58 (1998) 6506–6522.

[45] Y. B. Kim, C. F. Hempstead, A. R. Strnad, Critical persistent currents in hard superconductors, Phys. Rev. Lett. 9 (1962) 306–309.

[46] Z. Xu, R. Lewin, A. M. Campbell, D. A. Cardwell, H. Jones, Theoretical simulation studies of pulsed field magnetisation of (RE)BCO bulk superconductors, J. Phys.: Conf. Ser. 234 (2010) 012049.

[47] Z. Xu, R. Lewin, A. M. Campbell, D. A. Cardwell, H. Jones, Simulation studies on the magnetization of (RE)BCO bulk superconductors using various split-coil arrangements, Supercond. Sci. Technol. 25 (2012) 025016.

[48] A. M. Campbell, A new method of determining the critical state in superconductors, Supercond. Sci. Technol. 20 (2007) 292.

[49] A. M. Campbell, The interaction distance between flux lines and pinning centres, J. Phys. C: Solid State Phys. 4 (1971) 3186.

[50] W. S. Seow, R. A. Doyle, J. D. Johnson, D. Kumar, R. Somekh, D. J. C. Walker, A. M. Campbell, The elastic regime of vortices in superconducting YBCO and multilayer YBCO/PrBCO films, Physica C 241 (1995) 71 – 82.

[51] A. M. Campbell, DC magnetisation and flux profile techniques, in: R. A. Hein, T. L. Francavilla, D. H. Liebenberg (Eds.), Magnetic Susceptibility of Superconductors and Other Spin Systems, Plenum Press, New York, 1991, pp. 129–155.

[52] A. Sanchez, C. Navau, Magnetic properties of finite superconducting cylinders. I. Uniform applied field, Phys. Rev. B 64 (2001) 214506.

[53] A. Sanchez, C. Navau, Critical-current density from magnetization loops of finite high-Tc superconductors, Supercond. Sci. Technol. 14 (2001) 444–447.

[54] F. M. Araujo-Moreira, C. Navau, A. Sanchez, Meissner state in finite superconducting cylinders with uniform applied magnetic field, Phys. Rev. B 61 (2000) 634–639.

[55] P. Laurent, J.-F. Fagnard, B. Vanderheyden, N. Hari Babu, D. A. Cardwell, M. Ausloos, P. Vanderbemden, An ac susceptometer for the characterization of large, bulk superconducting samples, Meas. Sci. Technol. 19 (2008) 085705.

[56] D. A. Cardwell, M. Murakami, M. Zeisberger, W. Gawalek, R. Gonzalez-Arrabal, M. Eisterer, H. W. Weber, G. Fuchs, G. Krabbes, A. Leenders, H. C. Freyhardt, X. Chaud, R. Tournier, N. Hari Babu, Round robin measurements of the flux trapping properties of melt processed Sm–Ba–Cu–O bulk superconductors, Physica C 412-414, Part 1 (2004) 623 – 632.

[57] R. Gonzalez-Arrabal, M. Eisterer, H. W. Weber, Study of inhomogeneities in the flux density distribution of big monolithic (RE)$Ba_2Cu_3O_{7-\delta}$ melt-textured superconductors, J. Appl. Phys. 93 (2003) 4734–4738.

[58] I.-G. Chen, J. Liu, R. Weinstein, K. Lau, Characterization of $YBa_2Cu_3O_7$, including critical current density J_c, by trapped magnetic field, J. Appl. Phys. 72 (1992) 1013–1020.

[59] G. P. Lousberg, J.-F. Fagnard, J. G. Noudem, M. Ausloos, B. Vanderheyden, P. Vanderbemden, Measurement of the magnetic field inside the holes of a drilled bulk high-T_c superconductor, Supercond. Sci. Technol. 22 (2009) 045009.

[60] G. P. Lousberg, J.-F. Fagnard, E. Haanappel, X. Chaud, M. Ausloos, B. Vanderheyden, P. Vanderbemden, Pulsed-field magnetization of drilled bulk high-temperature superconductors: flux front propagation in the volume and on the surface, Supercond. Sci. Technol. 22 (2009) 125026.

[61] A. Gurevich, H. Küpfer, Time scales of the flux creep in superconductors, Phys. Rev. B 48 (1993) 6477–6487.

[62] Y. Mawatari, Magnetic field distributions around superconducting strips on ferromagnetic substrates, Phys. Rev. B 77 (2008) 104505.

[63] A. Sanchez, N. Del-Valle, C. Navau, D.-X. Chen, Influence of magnetic substrate in the transport critical current of superconducting tapes, Appl. Phys. Lett. 97 (2010) 072504.